Current Transformer-Based Power Supply for Pulse Encoders on Motor Power Lines in Adjustable Speed Drive Systems

Takumi Nakagaki, Masamichi Yamaguchi, Hiroki Watanabe, Yuki Nakata, Jun-ichi Itoh,
*Takeshi Kiribuchi **Shigeo Morimoto
Nagaoka University of Technology/ *OMRON Corporation/ **Osaka Metropolitan University
1603-1 Kamitomioka-machi, Nagaoka, Niigata, Japan
Tel.: +81 / (258) – 47.9533.
E-Mail: s235004@stn.nagaokaut.ac.jp, m_yamaguchi@stn.nagaokaut.ac.jp, hwatanabe@vos.nagaokaut.ac.jp, ynakata@vos.nagaokaut.ac.jp, itoh@vos.nagaokaut.ac.jp
URL: http://itohserver01.nagaokaut.ac.jp/itohlab/jp/index.html

Keywords

«DC Power Supply», «Transformer», «Sensor», «Permanent magnet motor», «DC-DC converter».

Abstract

This paper proposes a novel power supply system for an encoder in motor drive systems. The proposed system eliminates the need for a dedicated power supply cable for the encoder by utilizing a current transformer connected to the load motor. A design method for the current transformer is presented, considering its operation under non-linear loads and variable frequencies. The design process is simplified by modeling the diode rectifier as an equivalent voltage source. The validity of the proposed design is verified through experiments, demonstrating that the output voltage closely matches the design values. Additionally, a DC-DC converter is implemented at the output side of the diode rectifier to stabilize the output voltage. Experimental results confirm voltage stabilization across the entire operating range on the N-T map.

Introduction

Permanent magnet synchronous motors (PMSMs) are widely used in industrial applications due to their high efficiency and wide speed range. Typically, an encoder is required to detect the rotor position and rotational speed for precise PMSM control. The encoder requires both a power supply cable and a signal cable between the power converter and the encoder. However, in multi-motor systems, the complexity and cost associated with the power supply cable increase significantly.

To address this issue, several sensorless drive systems that eliminate the need for cables have been proposed [1-3]. Ref. [1] introduces a sensorless control method employing an integral adaptive observer based on a mathematical model of a PMSM. Additionally, a position control approach for servo systems utilizing feedback error learning is presented in [2]. Moreover, an extended observer designed for dual three-phase PMSMs with overmodulation is proposed in [3]. However, these sensorless drive systems face limitations in improving PMSM control accuracy.

In contrast, alternative approaches focus on reducing cable requirements while still an encoder [4-5]. Ref. [4] proposes a method to reduce signal cables by utilizing Power Line Communication (PLC), eliminating the need for a separate signal cable between the encoder and the controller. However, the power supply cable for the encoder remains necessary when using PLC. A battery-less encoder, which derives power from motor rotation energy, has also been introduced to eliminate the power supply cable [5]. However, this approach increases the overall system cost.

Another approach eliminates the encoder's power supply cable by sourcing power from the motor power line [6]. Ref. [6] employs a current transformer connected in series with the power line of the load motor. However, the power supply system in [6] does not address AC-DC conversion, which is required to provide stable DC power for the encoder. Furthermore, it does not clarify the design considerations for the current transformer under non-linear loads and variable frequency conditions.

This paper proposes a power supply system for encoders using a current transformer in motor drive systems. A design methodology for a current transformer in a three-phase system with

a diode rectifier is investigated. The three-phase system employs a diode rectifier to supply DC power to the encoder. The originality of the proposed method lies in its design approach, which linearizes the non-linear load characteristics of the diode rectifier. Furthermore, a DC-DC converter is incorporated at the output side of the diode rectifier to ensure voltage stabilization across the entire operating range on the N-T map of the PMSM.

Circuit configuration and equivalent circuit of the power supply system for the encoder

Circuit configuration

Fig. 1 shows the system configuration of the power supply system for the encoder. The primary side of the current transformer is connected to the power line of the three-phase motor to extract the drive power of the encoder. Thus, the operation frequency of the current transformer is the same as the frequency of the motor power line. The secondary side of the current transformer has the three-phase diode rectifier. The diode rectifier supplies the DC voltage to the encoder.

N-T characteristics of the power supply system for the encoder

Fig. 2 shows the N-T characteristics of the load motor with the characteristics of the power supply system for the encoder. The proposed system operates in three areas based on the motor torque and the rotation speed.

In area A, the motor torque and the rotation speed are sufficient for the encoder power supply. Thus, a current superimposition is not needed in the area A.

In area B, the motor torque is not sufficient because the motor current is low. Thus, a current superposition on the d-axis with only DC components is required for the encoder power supply. The amplitude of the DC components is determined by an output voltage difference between a measured value and a desired value.

On the other hand, area C is defined as the range of rotation speed within 0.1p.u. in this paper. The rotation speed is too low for the encoder power supply in area C. Thus, the required current superposition is not only DC components but also AC components on the d-axis. The AC component amplitude is determined by the output

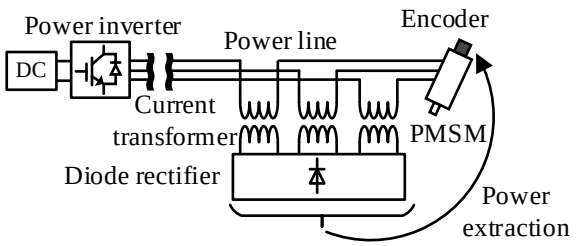

Fig.1. Configuration of power supply system with three-phase diode rectifier for encoder.

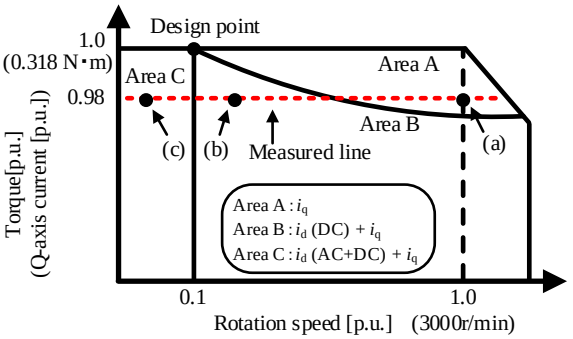

Fig. 2. N-T map of the PMSM with power supply system for the encoder.

voltage difference between the measured value and the desired value.

Then, the motor current exceeds the rated current because of the AC component of the d-axis current is superimposed on the rated value of the motor current. In particular, the superimposition of the d-axis current is maximum when the rotation speed is close to zero. The d-axis current is 1.0p.u. because only the AC component is supplied to the encoder in the conditions. Thus, the maximum motor current is 1.41p.u..

The maximum frequency of the AC component is defined as a fundamental frequency of the load motor. The minimum frequency is also defined as the cut-off frequency of the current controller. The frequency of the AC component is set at 200-Hz, which is 1/10 of a cut-off frequency in this paper.

Equivalent conversion of the diode rectifier

Fig. 3(a) shows the single-phase equivalent circuit of the proposed system in Fig. 1. The output of the diode rectifier is expressed as a voltage source because of the large capacitor connected to the output of the diode rectifier.

Fig. 3(b) shows the operation waveforms of the proposed system in Fig. 3(a). The input voltage of the diode rectifier is a square wave because the

input current of the diode rectifier is sinusoidal, as the system shown in Fig. 1. The current transformer is designed based on the motor current and the output characteristics. Then, the nonlinearity of the diode rectifier increases the complexity of the current transformer design.

Thus, the equivalent linear model of the diode rectifier is required to simplify the current transformer design.

Ref. [7] shows the equivalent resistance model of the diode rectifier with a current source drive and a large smoothing capacitor. Then, the forward voltage of the diode is not considered in modeling the equivalent resistance. Thus, the output DC voltage should be large sufficiently relative to the forward voltage of the diode in [7].

In contrast, the power supply system for the encoders requires the consideration of the forward voltage in the diodes due to the low DC voltage.

The input voltage of the diode rectifier v_{din} is expressed as

$$v_{\mathrm{din}} = \begin{cases} V_{\mathrm{o}} + 2V_{\mathrm{f}} \ldots (i_{\mathrm{din}} \geq 0) \\ -V_{\mathrm{o}} - 2V_{\mathrm{f}} \ldots (i_{\mathrm{din}} < 0) \end{cases} \quad \ldots\ldots\ldots\ldots\ldots\ldots (1),$$

where V_{o} is the output voltage for the encoder, V_{f} is the forward voltage of the diode, and i_{din} is the input current of the diode rectifier. The fundamental component of the input voltage affects the active power. The input voltage of the diode rectifier $V_{\mathrm{din\_f}}$ is expressed as

$$V_{\mathrm{din\_f}} = \frac{4}{\pi}\left(V_{\mathrm{o}} + 2V_{\mathrm{f}}\right) \ldots\ldots\ldots\ldots\ldots\ldots (2).$$

The equivalent voltage of the single-phase diode rectifier $V_{\mathrm{eo\_sp}}$ based on (2) is given by

$$V_{\mathrm{eo\_sp}} = \frac{2\sqrt{2}}{\pi}V_{\mathrm{o}} + \frac{4\sqrt{2}}{\pi}V_{\mathrm{f}} \ldots\ldots\ldots\ldots\ldots\ldots (3).$$

Fig. 4(a) shows the equivalent circuit after the conversion of the single-phase diode rectifier in Fig. 4(a). The linearization of a single-phase diode rectifier is achieved by (3). Fig. 4(b) shows the equivalent circuit after the equivalent conversion of the three-phase diode rectifier. Two equivalent voltage sources are connected to the output of the three-phase diode rectifier, as shown in Fig. 4(b). Thus, each equivalent voltage in the three-phase diode rectifier is a half value of the single-phase diode rectifier because the output voltage of the three-phase diode rectifier is the same as the output voltage of the single-phase diode rectifier. Fig. 4(c) shows the one-phase equivalent circuit after conversion of the three-phase diode rectifier. The one-phase equivalent

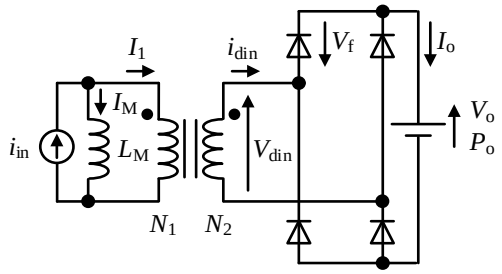

(a) Single-phase circuit of system with single-phase diode rectifier.

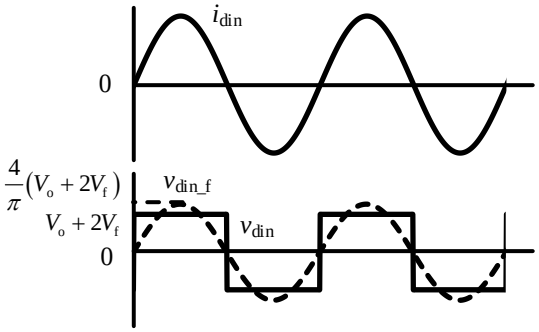

(b) Operation waveform.

Fig. 3. Single-phase equivalent circuit of proposed system.

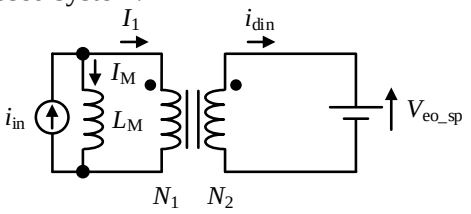

(a) Equivalent circuit after conversion of single-phase diode rectifier.

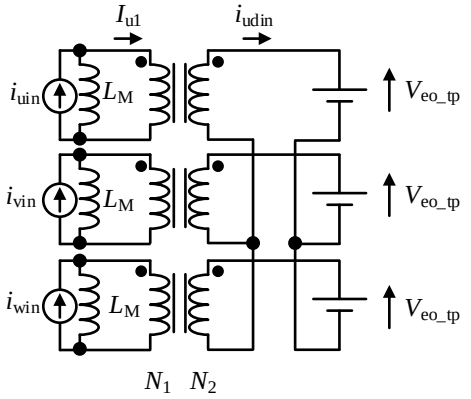

(b) Equivalent circuit for a phase after conversion of three-phase diode rectifier.

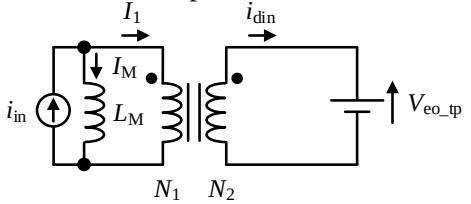

(c) One-phase equivalent circuit.

Fig. 4. One-phase equivalent circuit of system.

voltage of the three-phase diode rectifier V_{eo_tp} based on (3) is given by

$$V_{eo\_tp} = \frac{\sqrt{2}}{\pi} V_o + \frac{2\sqrt{2}}{\pi} V_f \quad \text{.....(4).}$$

The design of current transformer

Fig. 5 shows the design flowchart of the proposed current transformer. The current transformer is designed based on the motor current, output voltage, output power, and current ratio.

First, the RMS value of the input current of the diode rectifier I_{din} is calculated based on the output voltage and power. The input current of the diode rectifier I_{din} is expressed by

$$I_{din} = \frac{\pi}{3\sqrt{2}} \frac{P_o}{V_o} \quad \text{.....(5),}$$

where P_o is the output voltage for the encoder.

Second, the magnetic core is selected based on the area product method using the window area S_w and the effective cross-section area A_e [8]. The relationship between the window area Sw and the effective cross-section area A_e is expressed as

$$S_w A_e \geq \frac{V_{eo\_tp} I_{din}}{J \Delta B f K_u} \quad \text{.....(6),}$$

where J is the permissible current density of the windings, ΔB is the peak-to-peak of the flux density of the core, f is the frequency of the motor current, and K_u is the window utilization factor. The cores are selected from the cores which satisfy (6) with an additional space.

Third, the turn number of the transformer is calculated by core characteristics from (6). The turn ratio n is defined as the ratio of the turn number of the primary side N_1 to the turn number of the secondary side N_2. The turn ratio n is expressed as

$$n = \frac{N_1}{N_2} = \frac{I_{din}}{I_1} \quad \text{.....(7),}$$

where I_1 is the primary side current. The magnetizing current I_M is calculated from the relationship between the input current and the magnetizing current. The magnetizing current I_M is expressed as

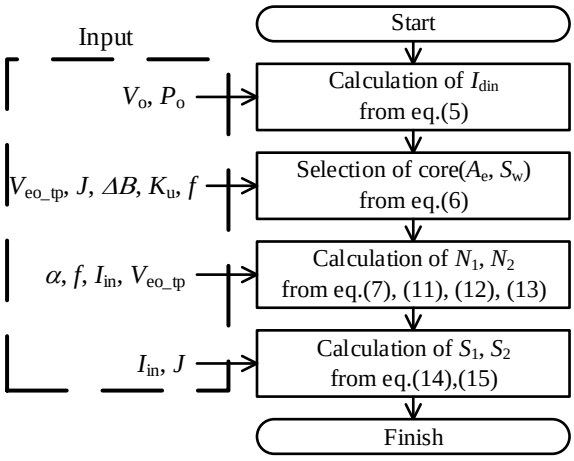

Fig. 5. Design a flowchart for a current transformer.

$$I_M = \frac{\frac{n^2 V_{eo\_tp}}{I_{din}}}{\sqrt{(2\pi f L_M)^2 + \left(\frac{n^2 V_{eo\_tp}}{I_{din}}\right)^2}} I_{in} \quad \text{.....(8),}$$

where L_M is the magnetizing inductance, and I_{in} is the RMS value of the input current. The relationship of each current based on Kirchhoff's current law is expressed as

$$I_{in}^{\ 2} = I_M^{\ 2} + I_1^{\ 2} \quad \text{.....(9).}$$

The current ratio α is defined as the ratio of the magnetizing current I_M to the input current I_{in}. The current ratio α is expressed as

$$\alpha = \frac{I_M}{I_{in}} \quad \text{..... (10).}$$

The turn ratio n of the current transformer is represented by substituting (9) and (10) into (7) as

$$n = \frac{1}{\sqrt{1-\alpha^2}} \frac{I_{din}}{I_{in}} \quad \text{..... (11).}$$

The magnetizing inductance L_M is calculated based on (8) and (10) by

$$L_M = \frac{n^2 V_{eo\_tp}}{2\pi f I_{din}} \sqrt{\left(\frac{1}{\alpha}\right)^2 - 1} \quad \text{..... (12).}$$

The turn number of the primary side is derived to obtain the magnetizing inductance calculated on (12). The magnetizing inductance is given by the magnetic reluctance and turn numbers. Thus, the turn number of the primary side is expressed as

$$N_1 = \sqrt{\frac{l_e L_M}{\mu_e A_e}} \quad \text{.....(13),}$$

where l_e is the length of the magnetic path in the core and μ_e is the effective magnetic permeability of the core.

Finally, the cross-section area of the windings S_1 and S_2 are selected so that the current density of the winding does not exceed the permissible current density of the windings J. The cross-section area of the windings S_1 and S_2 is expressed as

$$S_1 = \frac{I_{in}}{J} \quad \text{.....(14),}$$

$$S_2 = \frac{I_{din}}{J} \quad \text{.....(15).}$$

Table 1 shows the design conditions for the current transformer. The parameters of the PMSM used are a rated output of 100 W, a rated speed of 3000 r/min (1.0p.u.), and a rated current of 1.5 A (1.0p.u.). The current transformer is designed with a minimum frequency of 25-Hz(300 r/min) in this consideration.

Fig. 6 shows the overview of the prototype of the current transformer. A Cut core is used with a width of 62 mm and a height of 35 mm.

Table 2 shows the parameters of the prototype current transformer according to the proposed flowchart. The difference between each magnetizing inductance is slight. The maximum error ratio between the theoretical and measured values of the magnetizing inductance is 36.4%. The main cause of the error is the difference in the effective permeability of the core between the prototype and the design.

Fig. 7 shows the circuit configuration for the verification of a single current transformer. The load resistance R_{sp} is calculated from V_{eo_tp} and (5) in order to verify the validity of the proposed design of the current transformer. The load resistance for one phase R_{sp} is expressed as

$$R_{sp} = \frac{V_{eq\_tp}}{I_{din}} = \frac{6}{\pi^2}\frac{V_o^2}{P_o} + \frac{12}{\pi^2}\frac{V_o V_f}{P_o} \quad \text{.....(16).}$$

This paper applied a load resistance of 75.4 Ω based on the conditions in Table 1. In addition, the current transformer for V-phase is used to verify the experiment of the single current transformer. An AC power supply is used as the current source instead of the motor current in the experiments.

Fig. 8 shows the operation waveform of the single current transformer. The magnetizing current is 0.56 A based on the RMS value of the input voltage for the current transformer v_{in}. The magnetizing inductance of V-phase is shown in Table 2. The current ratio α is 0.37, which is an error of 7.5%. The cause of the error is the leakage inductance, winding resistance, and the difference in the magnetizing inductance between the design and the prototype of the current transformer. The large value of the magnetizing inductance affects the increase in the output current. However, the errors of the leakage inductance and the winding resistance affect the decrease in the output current. Thus, the error of the current ratio α is suppressed to 7.0%.

Table 1. Design specifications of current transformer.

Parameters	Symbol	Value
Motor current RMS and frequency	I_{in}, f	1.5 A_{RMS} 25 Hz
Output voltage and power	V_o, P_o	10 $V_{Avg.}$ 1 $W_{Avg.}$
Voltage drop of diode	V_f	1.2 V
Window utilization factor	K_u	0.5 -
The ratio of magnetizing current to primary-side current	α	0.4 -
permissible current density	J	4 A/mm^2
peak-to-peak of the flux density	ΔB	1.2 T

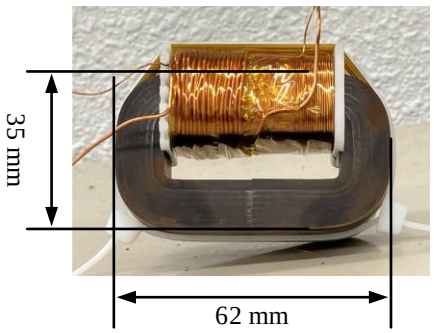

Fig. 6. Appearance of created current transformer.

Table 2. Parameter of designed current transformer.

Parameters	Symbol	Value		
		Calculation	Measurement	
Number of turns	$N_1 N_2$	17/316	17/316	turns
Magnetizing inductance	L_M	3.54	U 4.80	mH
			V 4.79	mH
			W 4.83	mH
Window area of the core	S_w	5.20	—	cm^2
Effective cross-section of the core	A_e	2.64	—	cm^2
Effective relative magnetic permeability of the core	μ_e	—	5100	—

Experimental results

Fig. 9 shows the configuration of the experimental tests. A DC-DC converter is connected at the output side of the diode rectifier to stabilize the output voltage against frequency and load fluctuations. The DC-DC converter stabilizes the output voltage using PI control. The smoothing capacitance is 470 μF. The encoder is simulated as a load resistor of 100 Ω.

Fig. 10 shows the output voltage characteristics with the variable speed under a torque of 0.98p.u.. The output voltage decreases due to a rotational speed decreasing without d-axis current superimposition. The output voltage characteristic indicates that the output power is also decreased in the low speed range. On the other hand, the output voltage is constant even in the low-speed range with d-axis current superimposition.

Fig. 11(a) shows the experimental waveform in area A (3000 r/min). A command value of the q-axis current is only 2.08 A in area A, whereas an output voltage achieves 10.0 V as the designed value without superimposing the d-axis current.

Fig. 11(b) shows the experimental waveform in area B (450 r/min). The desired output voltage is obtained by the superimposing d-axis current of -0.37 A. The output voltage without the superimposing d-axis current falls below 10.0 V in area B as shown in Fig. 10. Thus, the result demonstrates that the d-axis current superposition is effective to stabilize the output voltage.

Fig. 11(c) shows the experimental waveform in area C (60 r/min). The output voltage achieves designed value by superimposing an AC component on the d-axis current. The command value of q-axis current is 2.08 A and d-axis current is -0.42 A. Moreover, the d-axis current amplitude is 2.73 A, and the frequency is 200 Hz. The output voltage without the superimposing d-axis current falls below 10.0 V in area C as shown in Fig. 10.

The output voltage has a ripple, which is six times the frequency of the load motor current. The cause of the voltage ripple is an overmodulation of the output voltage control in the DC-DC converter. The design of the current transformer does not consider margin of the output voltage in this paper. Thus, the input current of the DC-DC converter is insufficient in the case of low-speed condition. As a result, the voltage control in the DC-DC converter becomes the overmodulation.

The motor current is 1.96 A (1.31p.u.) at the operating point shown in Fig. 11(c). Then, an overheating of the motor may occur in the case of the motor current exceeds the rated value. The overheating can be avoided by improving the design method of the current transformer and intermittent operation of the encoder power supply.

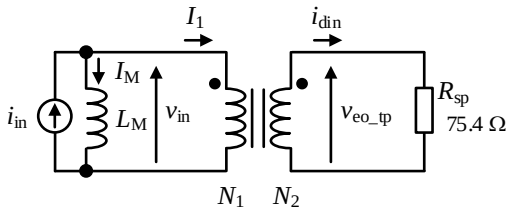

Fig. 7. Configuration of experimental circuit for single current transformer.

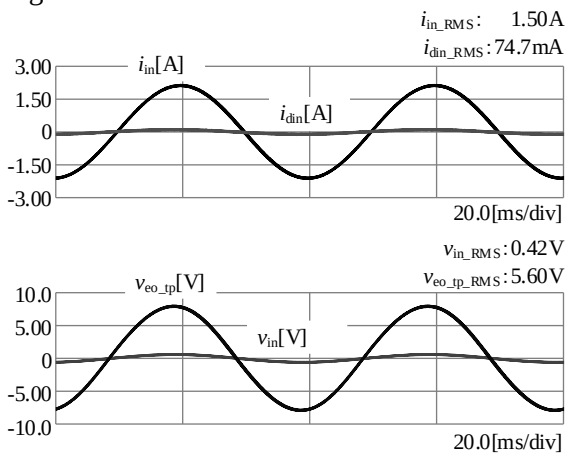

Fig. 8. Experimental results of power supply through single current transformer with design value.

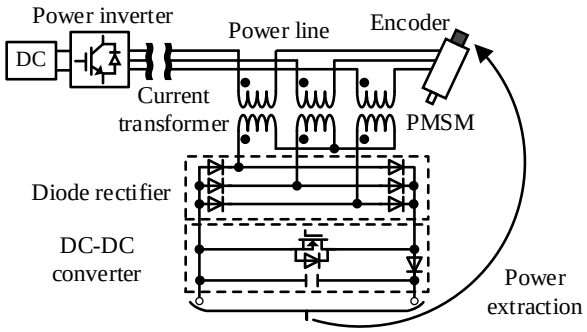

Fig. 9. Configuration of power supply system with three-phase diode rectifier for encoder.

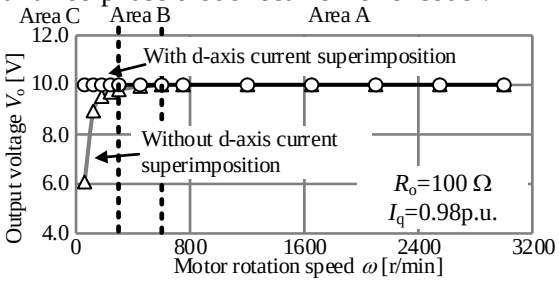

Fig. 10. Speed characteristics at 0.98p.u. torque.

Conclusion

This paper proposed a novel power supply system for encoders in motor drive systems using current transformers. Additionally, a design methodology for a current transformer in an encoder power supply system was presented. The validation of a single current transformer demonstrated the effectiveness of the proposed design approach. Experimental results confirmed that the desired voltage was achieved across the entire operating range on the N-T map through the superimposition of d-axis currents. Furthermore, the output voltage was stabilized using a DC-DC converter under varying motor rotation speeds.

Future work will focus on further improving the d-axis current superimposition method and refining the current transformer design methodology.

References

[1]. Z. Wang, X. Zhu, and W. Nie, “Sensorless Control Strategy for Permanent Magnet Synchronous Motor Integral Adaptive Observer”, IEEJ Journal of Industry Applications, Vol. 14, No. 1, pp. 120-130, 2025.

[2]. N. Kawamura, S. Inoue, T. Zanma, K. Kondo, K. Koiwa, K. Liu, and M. Shibata, “Feedback Error Learning-Based Position Control in Position-Sensorless Positioning Servo Systems for IPMSMs”, IEEJ Journal of Industry Applications, Vol. 12, No. 4, pp. 816-825, 2023.

[3]. K. Imai, S. Doki, K. Kondo, and Y. Aoki, “Extended EMF Observer of Dual Three-Phase Permanent Magnet Synchronous Motor Operable in Overmodulation Drive”, IEEJ Journal of Industry Applications, Vol. 12, No. 5, pp. 901-913, 2023.

[4]. M. V. Ribeiro, Â. Camponogara, Mateus De L. Filomeno, T. R. Oliveira, T. F. Moreira, S. Galli, and H. V. Poor, “Seamless Connectivity: The Power of Integrating Power Line and Wireless Communications”, in IEEE Communications Surveys & Tutorials, Vol. 26, No. 1, pp. 1-40, 2024.

[5]. Y. Takemura, N. Fujinaga, A. Takebuchi, and T. Yamada, “Batteryless Hall Sensor Operated by Energy Harvesting From a Single Wiegand Pulse”, IEEE Trans. on Magnetics, Vol. 53, No.11, pp. 1-6, 2017.

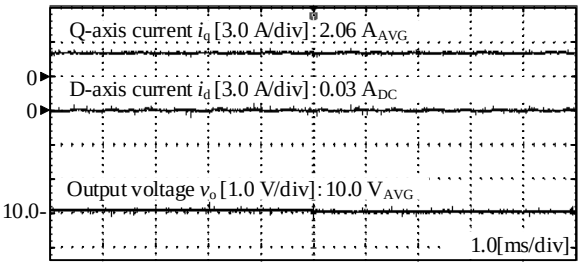

(a) Operating waveforms in area A(3000 r/min)

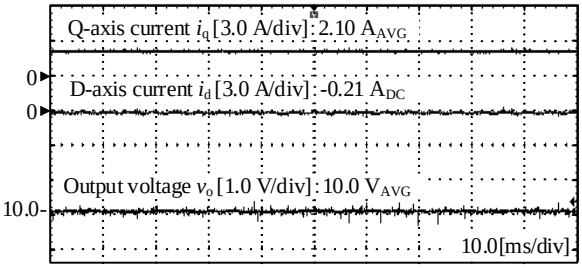

(b) Operating waveforms in area B(450 r/min)

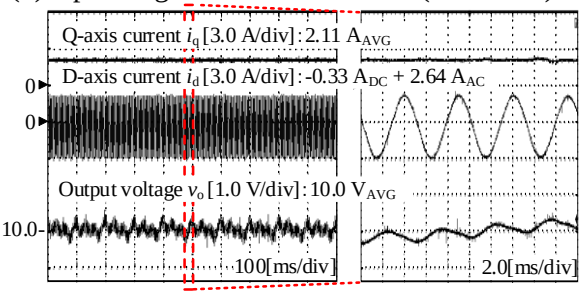

(c) Operating waveforms in area C(60 r/min)

Fig. 11. Operating waveforms in each superimposed area.

[6]. T. Kiribuchi, Y. Inoue, and S. Morimoto, “Secondary-Side Power Control Method of Power Superposition Using Single-Phase Transformer for Power Supply of Position Sensor in Permanent Magnet Synchronous Motor” 2023 25th European Conference on Power Electronics and Applications (EPE’23 ECCE Europe), pp.1-7, 2023.

[7]. R. L. Steigerwald, “A comparison of half-bridge resonant converter topologies”, IEEE Trans. on Power Electronics, Vol.3, No.2, pp.174-182, 1988.

[8]. W. T. Mclyman “Transformer and inductor design handbook”, Marcel Dekker Inc., 2004.